INTERNATIONAL JOURNAL FOR NUMERICAL METHODS IN FLUIDS
Int. J. Numer. Meth. Fluids 2004; **45**:365–389 (DOI: 10.1002/fld.702)

Stability and accuracy of a semi-implicit Godunov scheme for mass transport

Scott F. Bradford*,†,‡

Naval Research Laboratory, Image Science and Applications Branch, Code 7261, 4555 Overlook Ave. SW, Washington, DC 20375, U.S.A.

SUMMARY

Semi-implicit, Godunov-type models are adapted for solving the two-dimensional, time-dependent, mass transport equation on a geophysical scale. The method uses Van Leer's MUSCL reconstruction in conjunction with an explicit, predictor–corrector method to discretize and integrate the advection and lateral diffusion portions of the governing equation to second-order spatial and temporal accuracy. Three classical schemes are investigated for computing advection: Lax-Wendroff, Warming-Beam, and Fromm. The proposed method uses second order, centred finite differences to spatially discretize the diffusion terms. In order to improve model stability and efficiency, vertical diffusion is implicitly integrated with the Crank–Nicolson method and implicit treatment of vertical diffusion in the predictor is also examined. Semi-discrete and Von Neumann analyses are utilized to compare the stability as well as the amplitude and phase accuracy of the proposed method with other explicit and semi-implicit schemes. Some linear, two-dimensional examples are solved and predictions are compared with the analytical solutions. Computational effort is also examined to illustrate the improved efficiency of the proposed model. Copyright © 2004 John Wiley & Sons, Ltd.

KEY WORDS: semi-implicit; mass transport; Godunov; finite volume; stability; accuracy

INTRODUCTION

Godunov-type finite volume methods have become increasingly popular for modelling advection dominated mass transport. Such schemes use either cell-centred or cell-vertex values of mass to construct upwind-biased advective fluxes at cell boundaries. Diffusion terms are generally treated with space-centred finite differences and the governing equation is typically integrated in time with an explicit method. On unstructured grids, diffusion may be discretized in a finite volume framework [1], or a finite element approach [2], while Zwart *et al.* [3] developed an integrated space-time finite volume discretization of time to conserve mass in

*Correspondence to: Scott F. Bradford, Naval Research Laboratory, Image Science and Applications Branch, Code 7261, 4555 Overlook Avenue SW, Washington, DC 20375, U.S.A.
†E-mail: bradford@ccf.nrl.navy.mil
‡Research Scientist.

Received 14 July 2003
Revised 15 January 2004

moving boundary problems. Higher accuracy is obtained by reconstructing cell-average data with polynomials prior to computing the advective fluxes and integrating the governing equation with an explicit, multi-step Runge–Kutta (RK) method. Flux or slope limiting is often employed to suppress the development of spurious oscillations that accompanies higher spatial accuracy.

These schemes are popular because of their mass conserving properties and ability to accurately compute waves and sharp fronts that are free of numerical oscillations. Such models are also efficient, but because of their explicit character, they must obey the Courant condition to maintain stability of the numerical solution. However, the vertical scale in rivers, estuaries, and other geophysical environments is much smaller than the lateral scales. In addition, mass transport may be dominated by turbulent mixing or chemical and biological reactions, as opposed to advection. Under these conditions, the source or vertical diffusion terms may become stiff and initiate numerical instability. The explicit treatment of such terms forces a further reduction of the time step below that dictated by the Courant condition and hence reduces model efficiency. In such cases, it is desirable to treat diffusion and stiff source terms implicitly to enhance model stability, while treating advection and non-stiff source terms explicitly to maintain good phase accuracy and minimize computational expense. There has been much research and application of such semi-implicit schemes of which there are two general approaches.

The first approach is to use splitting or fractional steps in which the stiff and non-stiff portions of the equation are split and solved independently in a sequential manner. Leveque and Yee [4] developed a split version of the semi-implicit MacCormack scheme for the one-dimensional advection equation with a stiff source term. This scheme consists of a stiff term, implicit integration step, a non-stiff step with the explicit MacCormack scheme, and a final stiff implicit integration step.

The second approach is to simultaneously integrate stiff and non-stiff terms in a unified manner. Moin and Kim [5] used this approach to solve the Navier–Stokes equations by applying the Crank–Nicholson method to the pressure and viscous terms and the explicit, second-order Adams-Bashforth method to the remaining terms. Verwer *et al.* [6] solved the advection–diffusion-reaction equation by discretizing the time derivative with a second-order backward difference and implicitly integrating vertical diffusion and stiff reaction terms with the first-order backward Euler method. Advection and non-stiff reaction terms were explicitly integrated by linearly extrapolating the concentration from the previous two time levels. Knoth and Wolke [7] improved this model by treating advection with high order accurate RK methods while Zhong [7] developed second and third-order schemes based on RK methods that treat non-stiff terms explicitly and stiff terms implicitly. Bell *et al.* [9] developed a second order, semi-implicit Godunov method for the Navier–Stokes equations that utilized an explicit second-order RK method to integrate the advection terms and the Crank–Nicolson method to integrate the viscous terms.

In this study, another form of the semi-implicit Godunov method is proposed. The method proposed by Bell *et al.* [9] treated diffusion in all directions implicitly, which requires the inversion of large sparse matrices in multidimensional problems. However, in geophysical problems, the lateral diffusion terms are typically much smaller than the vertical terms and therefore implicitly integrating all diffusion terms is unnecessarily expensive. In this paper, a simpler semi-implicit Godunov method that is specifically tailored for geophysical applications involving the transport of mass in rivers and coastal waters is proposed. This method treats

only vertical diffusion implicitly. Accuracy, stability, and computational demand are compared with the fully explicit Godunov method as well as other semi-implicit Godunov methods.

SEMI-DISCRETE ANALYSIS

The proposed time stepping scheme is first analysed independently of the spatial discretization. For this purpose, a simple test problem is examined of the form

$$\frac{\mathrm{d}c}{\mathrm{d}t} = (\lambda_\mathrm{n} + \lambda_\mathrm{s})c \tag{1}$$

where λ_n and λ_s represent non-stiff and stiff complex source terms, respectively.

The proposed semi-implicit time scheme for Equation (1) is

$$c^{n+1} = c^n + \Delta t \left(\lambda_\mathrm{n} c^{n+1/2} + \frac{\lambda_\mathrm{s}}{2} (c^{n+1} + c^n) \right) \tag{2}$$

where n is the time level and $c^{n+1/2}$ is a predictor value that is computed as

$$c^{n+1/2} = c^n + \frac{\Delta t}{2} [\lambda_\mathrm{n} c^n + \lambda_\mathrm{s} (w c^{n+1/2} + \tilde{w} c^n)] \tag{3}$$

The term w varies from 0 for an explicit method to 1 for an implicit method and $\tilde{w} = 1 - w$. If the following definitions are made,

$$\begin{aligned} x &= \lambda_\mathrm{n} \Delta t = a + bI \\ y &= \frac{\lambda_\mathrm{s} \Delta t}{2} = |y|(\cos\phi + \sin\phi I) \end{aligned} \tag{4}$$

(where $I = \sqrt{-1}$) then the semi-implicit integration of Equation (1) results in the following expression for the amplification factor $G = c^{n+1}/c^n$,

$$G = \frac{(1 + |y|\cos\phi + a\tilde{a} - b\tilde{b})(1 - |y|\cos\phi)}{(1 - |y|\cos\phi)^2 + (|y|\sin\phi)^2} + \frac{|y|\sin\phi + b\tilde{a} + a\tilde{b}}{(1 - |y|\cos\phi)^2 + (|y|\sin\phi)^2} I \tag{5}$$

where

$$\begin{aligned} \tilde{a} &= \frac{(1 + \frac{a}{2} + \tilde{w}|y|\cos\phi)(1 - w|y|\cos\phi) - (\frac{b}{2} + \tilde{w}|y|\sin\phi) w|y|\sin\phi}{(1 - w|y|\cos\phi)^2 + (w|y|\sin\phi)^2} \\ \tilde{b} &= \frac{(1 + \frac{a}{2} + \tilde{w}|y|\cos\phi) w|y|\sin\phi - (\frac{b}{2} + \tilde{w}|y|\sin\phi)(1 - w|y|\cos\phi)}{(1 - w|y|\cos\phi)^2 + (w|y|\sin\phi)^2} \end{aligned} \tag{6}$$

The stability region is defined as the region in the complex plane where $|G| \leqslant 1$ for all y and plotted as a function of x. The search space for y is defined as $\pi + \gamma \leqslant \phi \leqslant \pi - \gamma$ and $|y| \to \infty$. Figure 1 shows plots of the stability region for $w = 0$ and different values of γ and reveals that the stability region becomes smaller as γ grows. Figure 1 also shows the stability region for $w \geqslant \frac{1}{2}$, which does not vary with γ. In this case, the stability region is much larger,

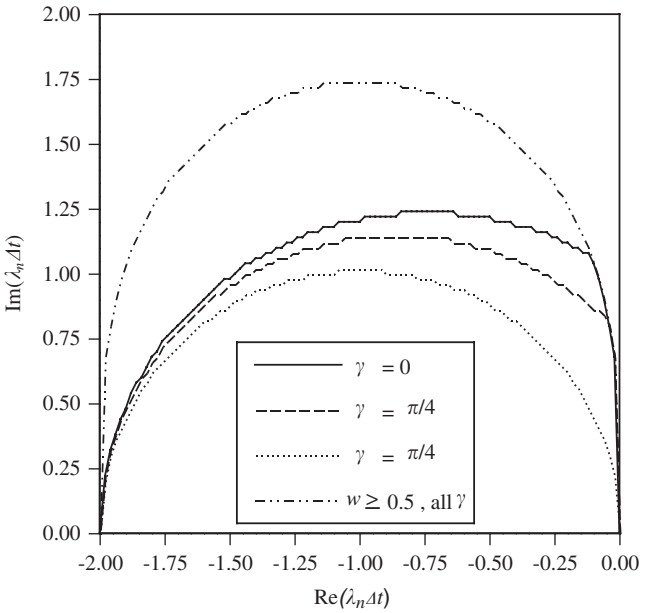

Figure 1. Stability region for the proposed semi-implicit method.

which indicates the greater potential stability that accompanies the implicit calculation of the predictor when coupled with a suitable spatial discretization.

For comparison, consider the Adams–Bashforth–Crank–Nicolson (ABCN) method proposed by Moin and Kim [5] for Equation (1), which is

$$c^{n+1} = c^n + \frac{x}{2}(3c^n - c^{n-1}) + y(c^{n+1} + c^n) \tag{7}$$

The resulting equation for G is

$$(1-y)G^2 - \left(\frac{3x}{2} + y + 1\right)G + \frac{x}{2} = 0 \tag{8}$$

Substituting $G = e^{I\theta}$ where $0 \leqslant \theta \leqslant 2\pi$ into Equation (8) and solving for x yields

$$x = \frac{2A(1-3\cos\theta) - 6B\sin\theta}{(1-3\cos\theta)^2 + (3\sin\theta)^2} + \frac{2B(1-3\cos\theta) + 6A\sin\theta}{(1-3\cos\theta)^2 + (3\sin\theta)^2} I \tag{9}$$

where

$$\begin{aligned} A &= \cos\theta - \cos 2\theta + |y|[\cos(\phi+\theta) - \cos(\phi+2\theta)] \\ B &= \sin\theta - \sin 2\theta + |y|[\sin(\phi+\theta) + \sin(\phi+2\theta)] \end{aligned} \tag{10}$$

The stability region of this method is shown in Figure 2, which is seen to be smaller than for the proposed method. In addition, the region grows much smaller as γ increases.

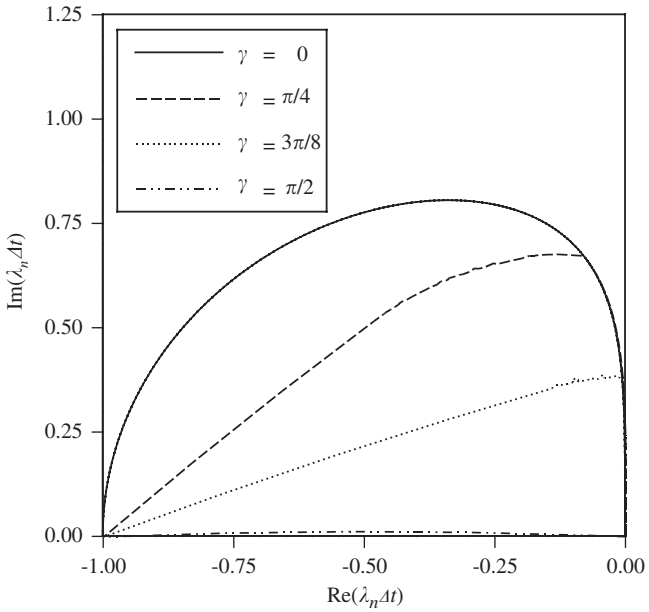

Figure 2. Stability region for the Adams–Bashforth–Crank–Nicolson (ABCN) method.

The additive, second-order Runge–Kutta (ASIRK-2) method developed by Zhong [8] and applied to Equation (1) results in the following expression:

$$c^{n+1} = \left(1 + \frac{(\frac{x}{2} - \frac{y}{24} + 1)(x+y)}{(1-\frac{y}{4})(1-\frac{y}{3})}\right) c^n \tag{11}$$

and the resulting equation for G is

$$G = 1 + \frac{A\tilde{A} + B\tilde{B}}{A^2 + B^2} + \frac{A\tilde{B} - B\tilde{A}}{A^2 + B^2} I \tag{12}$$

where

$$\begin{aligned} A &= \frac{|y|^2}{12}\cos 2\phi - \frac{7|y|}{12}\cos\phi + 1 \\ B &= \frac{|y|^2}{12}\sin 2\phi - \frac{7|y|}{12}\sin\phi \\ \tilde{A} &= \left(2 + a - \frac{|y|}{12}\cos\phi\right)\left(\frac{a}{2} + \frac{|y|}{2}\cos\phi\right) - \left(b - \frac{|y|}{12}\sin\phi\right)\left(\frac{b}{2} + \frac{|y|}{2}\sin\phi\right) \\ \tilde{B} &= \left(\frac{a}{2} + \frac{|y|}{2}\cos\phi\right)\left(b - \frac{|y|}{12}\sin\phi\right) + \left(2 + a - \frac{|y|}{12}\cos\phi\right)\left(\frac{b}{2} + \frac{|y|}{2}\sin\phi\right) \end{aligned} \tag{13}$$

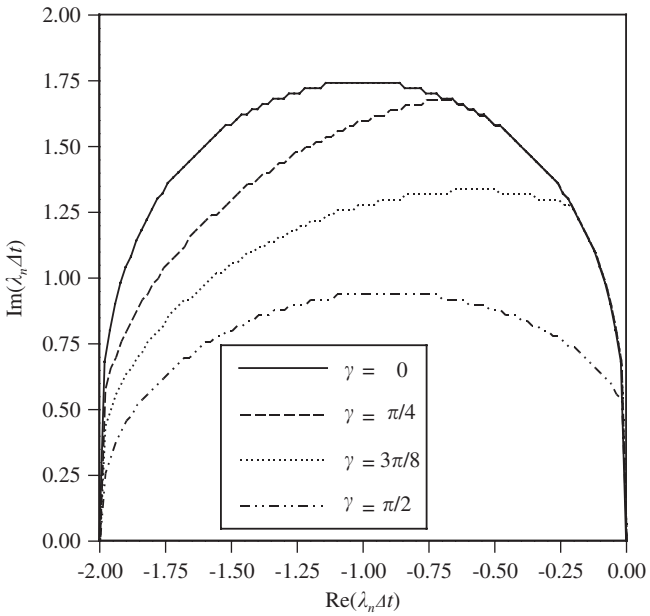

Figure 3. Stability region for the additive, semi-implicit, Runge–Kutta (ASIRK-2) method.

Figure 3 illustrates the stability region of this method for varying γ. Despite the fact that this method was designed to maximize stability, its stability region still shrinks as γ increases.

VON NEUMANN ANALYSIS AND NUMERICAL STABILITY

The proposed method is now applied to the linearized, two dimensional, advection–diffusion equation for an arbitrary scalar, c,

$$\frac{\partial c}{\partial t} + u\frac{\partial c}{\partial x} + v\frac{\partial c}{\partial y} = D_x\frac{\partial^2 c}{\partial x^2} + D_y\frac{\partial^2 c}{\partial y^2} \tag{14}$$

where the flow velocities u and v, as well as the turbulent diffusivities D_x and D_y, are constant.

Explicit method

First, a purely explicit Godunov-type scheme for solving Equation (14) is presented for the sake of comparison with semi-implicit methods. Such a second-order accurate scheme for solving the governing equation is

$$\begin{aligned} c_{j,k}^{n+1} = c_{j,k}^{n} &- \alpha_x(c_{j+1/2,k}^{n+1/2} - c_{j-1/2,k}^{n+1/2}) - \alpha_y(c_{j,k+1/2}^{n+1/2} - c_{j,k-1/2}^{n+1/2}) \\ &+ \beta_x(c_{j+1,k}^{n+1/2} - 2c_{j,k}^{n+1/2} + c_{j-1,k}^{n+1/2}) + \beta_y(c_{j,k+1}^{n+1/2} - 2c_{j,k}^{n+1/2} + c_{j,k-1}^{n+1/2}) \end{aligned} \tag{15}$$

where j and k denote the cell indices in the x and y directions, respectively, and n denotes the time level. The fractional subscripts denote cell faces, while the Courant numbers are defined as, $\alpha_x = u\Delta t/\Delta x$, $\alpha_y = v\Delta t/\Delta y$. The diffusion numbers are defined as $\beta_x = D_x\Delta t/\Delta x^2$, and $\beta_y = D_y\Delta t/\Delta y^2$. Furthermore, Δt is the time step and Δx and Δy are the grid spacings in the x and y directions, respectively.

This scheme utilizes predictor values of c at the $n+\frac{1}{2}$ time level that are computed as

$$c_{j,k}^{n+1/2} = c_{j,k}^n - \tfrac{1}{2}\left[\alpha_x \Delta_x c_{j,k} + \alpha_y \Delta_y c_{j,k} - \beta_x (c_{j+1,k}^n - 2c_{j,k}^n + c_{j-1,k}^n)\right. \tag{16}$$

$$\left. - \beta_y (c_{j,k+1}^n - 2c_{j,k}^n + c_{j,k-1}^n)\right] \tag{17}$$

The cell-average gradients of c, $\Delta_x c$ and $\Delta_y c$ are computed at time level n as

$$\begin{aligned} \Delta_x c_{j,k} &= \rho(c_{j+1,k}^n - c_{j,k}^n) + (1-\rho)(c_{j,k}^n - c_{j-1,k}^n) \\ \Delta_y c_{j,k} &= \rho(c_{j,k+1}^n - c_{j,k}^n) + (1-\rho)(c_{j,k}^n - c_{j,k-1}^n) \end{aligned} \tag{18}$$

where $0 \leqslant \rho \leqslant 1$. Selecting $\rho = 1$ yields the Lax-Wendroff (LW) method, $\rho = 0$ yields the Warming-Beam (WB) method and $\rho = \frac{1}{2}$ results in the Fromm scheme. Non-linear averages, termed slope limiters, are often used to prevent spurious oscillations from developing at discontinuities in c. Limiters typically use some combination of linear averages given by Equation (18) in regions of smooth c, but preserve solution monotonicity by adding dissipation in regions of steep gradients and ultimately becoming first-order accurate at solution extrema. Due to their non-linear nature, limiters are not examined in this study.

The cell face values of c are taken as the upwind values that are reconstructed following Van Leer's Monotone Upstream Scheme for Conservation Laws (MUSCL) [10] as

$$\begin{aligned} c_{j-1/2,k}^{n+1/2} &= c_{j-1,k}^{n+1/2} + \tfrac{1}{2}\Delta_x c_{j-1,k} \quad c_{j,k-1/2}^{n+1/2} = c_{j,k-1}^{n+1/2} + \tfrac{1}{2}\Delta_y c_{j,k-1} \\ c_{j+1/2,k}^{n+1/2} &= c_{j,k}^{n+1/2} + \tfrac{1}{2}\Delta_x c_{j,k} \quad c_{j,k+1/2}^{n+1/2} = c_{j,k}^{n+1/2} + \tfrac{1}{2}\Delta_y c_{j,k} \end{aligned} \tag{19}$$

A Von Neumann analysis of this method is performed by assuming that a separation of variables is valid and inserting the solution for a single harmonic of the form

$$c_{j,k}^n = g^n \mathrm{e}^{I(j\theta_x + k\theta_y)} \tag{20}$$

where θ_x and θ_y represent the harmonics in the x and y directions, respectively. Insertion of such expressions for each cell value into the discrete equation yields the following expression for the amplification factor, $G = g^{n+1}/g^n$,

$$\begin{aligned} G = {} & A_0 + A_1\cos\theta_x + A_2\cos\theta_y + A_3\cos 2\theta_x + A_4\cos 2\theta_y \\ & + A_5\cos(\theta_x - \theta_y) + A_6\cos(\theta_x + \theta_y) + [B_1\sin\theta_x + B_2\sin\theta_y \\ & + B_3\sin 2\theta_x + B_4\sin 2\theta_y + B_5\sin(\theta_x - \theta_y) + B_6\sin(\theta_x + \theta_y)]I \end{aligned} \tag{21}$$

with

$$
\begin{aligned}
A_0 &= 1 + \tfrac{3}{2}(\rho-1)(\alpha_x+\alpha_y) + \alpha_x\alpha_y(1-2\rho) + \frac{1-3\rho}{2}(\alpha_x^2+\alpha_y^2) \\
&\quad -2\beta_x - 2\beta_y + 3\beta_x^2 + 4\beta_x\beta_y + 3\beta_y^2 + (3\alpha_x\beta_x + 2\alpha_x\beta_y + 2\alpha_y\beta_x + 3\alpha_y\beta_y)(1-\rho) \\
A_1 &= \alpha_x[1+(2\rho-1)(\alpha_x+\alpha_y-1)] + 2\beta_x - 4\beta_x\beta_y - 4\beta_x^2 \\
&\quad + \alpha_x\beta_x(5\rho-4) + \alpha_x\beta_y(\rho-2) + 2\alpha_y\beta_x(\rho-1) \\
A_2 &= \alpha_y[1+(2\rho-1)(\alpha_x+\alpha_y-1)] + 2\beta_y - 4\beta_x\beta_y - 4\beta_y^2 \\
&\quad + 2\alpha_x\beta_y(\rho-1) + \alpha_y\beta_x(\rho-2) + \alpha_y\beta_y(5\rho-4) \\
A_3 &= \frac{\alpha_x(1-\rho)}{2}(\alpha_x + 2\beta_x - 1) + \beta_x^2 \\
A_4 &= \frac{\alpha_y(1-\rho)}{2}(\alpha_y + 2\beta_y - 1) + \beta_y^2 \\
A_5 &= (\alpha_x\beta_y + \alpha_y\beta_x)(1-\rho) - \rho\alpha_x\alpha_y + 2\beta_x\beta_y \\
A_6 &= (\alpha_x\alpha_y + \alpha_x\beta_y + \alpha_y\beta_x)(1-\rho) + 2\beta_x\beta_y \\
B_1 &= \alpha_x[(1-\rho)(\alpha_x+\alpha_y) + \beta_x(2+\rho) + (\beta_y-1)(2-\rho)] \\
B_2 &= \alpha_y[(1-\rho)(\alpha_x+\alpha_y) + (\beta_x-1)(2-\rho) + \beta_y(2+\rho)] \\
B_3 &= \frac{\alpha_x}{2}[(1-\alpha_x)(1-\rho) - 2\beta_x] \\
B_4 &= \frac{\alpha_y}{2}[(1-\alpha_y)(1-\rho) - 2\beta_y] \\
B_5 &= \alpha_y\beta_x - \alpha_x\beta_y \\
B_6 &= \alpha_x\alpha_y(\rho-1) - \alpha_x\beta_y - \alpha_y\beta_x
\end{aligned}
\tag{22}
$$

For numerical stability, $|G| \leqslant 1$ must be true for all $0 \leqslant \theta_x \leqslant \pi$ and $0 \leqslant \theta_y \leqslant \pi$. Numerical evaluation of Equation (21) indicates that when $\alpha_x = \alpha_y$, $\beta_x = \beta_y$, and $\theta_x = \theta_y = \pi$, $|G|$ is maximized for all three values of ρ examined in this study. In this case, maintaining stability requires

$$\beta_x + \beta_y < \tfrac{1}{2} \tag{23}$$

There are additional constraints on α that depend on the specific choice of ρ. Unfortunately, the WB method is also unstable for $\theta_x = \pi$ over a wide range of θ_y as well as for the symmetric cases $\theta_y = \pi$ and varying θ_x, which further reduces the maximum allowable α_x and α_y. In this case the additional constraint is

$$\alpha_x + \alpha_y \leqslant \min\left(1, 1 - 2(\beta_x+\beta_y) + \sqrt{1-2(\beta_x+\beta_y)}\right) \tag{24}$$

For the LW method, the following applies,

$$\alpha_x + \alpha_y \leqslant \sqrt{2(\beta_x + \beta_y)[2(\beta_x + \beta_y) - 1] + 1} \tag{25}$$

while for the Fromm method, the following must be obeyed,

$$\alpha_x + \alpha_y \leqslant 1 \tag{26}$$

However, the LW and Fromm methods also become unstable for $\theta_x = \theta_y = 0$. In this case G becomes

$$G = 1 + \rho(\alpha_x - \alpha_y)(\beta_x - \beta_y) \tag{27}$$

Schemes with $\rho > 0$ are unstable unless $\alpha_x \approx \alpha_y$ or $\beta_x \approx \beta_y$. Otherwise if $\alpha_x < \alpha_y$ then $\beta_x > \beta_y$ or if $\alpha_x > \alpha_y$ then $\beta_x < \beta_y$ must be maintained to preserve model stability. There are further cases in which the LW and Fromm schemes may be unstable including $\theta_x = 0$ with a wide range of $\theta_y > 0$ and the symmetric case $\theta_y = 0$, $\theta_x > 0$. These cases further restrict the stability of these methods and are not considered further here.

In many engineering applications, the computational mesh may be refined in areas of rapidly changing geometry in order to capture small scale flow features and minimize truncation errors. In addition, spatially and temporally varying diffusion coefficients from auxiliary turbulence models may be used to better model flow physics. Such actions yield small mesh spacings and possibly large local values of D_x and D_y and consequently, the constraint given by Equation (23) can severely restrict the allowable size of Δt required to preserve model stability. So although the explicit method is computationally expedient since it does not require matrix inversion, it is inefficient in the sense that a very small timestep may be required to maintain numerical stability. Therefore, the implicit treatment of diffusion is now investigated in an effort to ease this constraint on the time step.

Semi-implicit method 1

Advection is treated as before and an explicit predictor is computed as given by Equation (17). However, now diffusion is treated implicitly with the Crank–Nicholson method when computing the corrector as

$$\begin{aligned} c_{j,k}^{n+1} - \frac{\beta_x}{2}(c_{j+1,k}^{n+1} - 2c_{j,k}^{n+1} + c_{j-1,k}^{n+1}) - \frac{\beta_y}{2}(c_{j,k+1}^{n+1} - 2c_{j,k}^{n+1} + c_{j,k-1}^{n+1}) \\ = c_{j,k}^{n} - \alpha_x(c_{j+1/2,k}^{n+1/2} - c_{j-1/2,k}^{n+1/2}) - \alpha_y(c_{j,k+1/2}^{n+1/2} - c_{j,k-1/2}^{n+1/2}) \\ + \frac{\beta_x}{2}(c_{j+1,k}^{n} - 2c_{j,k}^{n} + c_{j-1,k}^{n}) + \frac{\beta_y}{2}(c_{j,k+1}^{n} - 2c_{j,k}^{n} + c_{j,k-1}^{n}) \end{aligned} \tag{28}$$

This is similar to the model proposed by Bell *et al.* [9] except that they treated cell-average gradients differently. When computing predictor values at a cell face, they used a centred

difference ($\rho = \frac{1}{2}$) to compute the gradient perpendicular to the face and an upwind difference ($\rho = 0$) to compute the gradient parallel to the face. However, this has no effect on the overall stability of the linear model as discussed below.

A Von Neumann analysis of this method yields

$$\begin{aligned}
&[1 + \beta_x(1 - \cos\theta_x) + \beta_y(1 - \cos\theta_y)]G \\
&\quad = A_0 + A_1\cos\theta_x + A_2\cos\theta_y + A_3\cos 2\theta_x + A_4\cos 2\theta_y \\
&\qquad + A_5\cos(\theta_x - \theta_y) + A_6\cos(\theta_x + \theta_y) + [B_1\sin\theta_x + B_2\sin\theta_y \\
&\qquad - A_3\sin 2\theta_x - A_4\sin 2\theta_y + B_3\sin(\theta_x - \theta_y) - A_6\sin(\theta_x + \theta_y)]I
\end{aligned} \tag{29}$$

where

$$\begin{aligned}
A_0 &= 1 + \frac{3(\rho-1)}{2}(\alpha_x + \alpha_y) + \frac{1-3\rho}{2}(\alpha_x^2 + \alpha_y^2) + (1-2\rho)\alpha_x\alpha_y \\
&\quad + \beta_x\left(\frac{3\alpha_x}{2} + \alpha_y - 1\right) + \beta_y\left(\alpha_x + \frac{3\alpha_y}{2} - 1\right) \\
A_1 &= (\alpha_x + \alpha_y - 1)[\alpha_x(2\rho - 1) - \beta_x] + \alpha_x(1 - \beta_x - \beta_y) \\
A_2 &= (\alpha_x + \alpha_y - 1)[\alpha_y(2\rho - 1) - \beta_y] + \alpha_y(1 - \beta_x - \beta_y) \\
A_3 &= \frac{\alpha_x}{2}[(\alpha_x - 1)(1-\rho) + \beta_x] \quad A_4 = \frac{\alpha_y}{2}[(\alpha_y - 1)(1-\rho) + \beta_y] \\
A_5 &= \tfrac{1}{2}(\alpha_x\beta_y + \alpha_y\beta_x) - \rho\alpha_x\alpha_y \quad A_6 = \tfrac{1}{2}(\alpha_x\beta_y + \alpha_y\beta_x) + (1-\rho)\alpha_x\alpha_y \\
B_1 &= \alpha_x[\rho - 2 + (1-\rho)(\alpha_x + \alpha_y) + \beta_x + \beta_y] \\
B_2 &= \alpha_y[\rho - 2 + (1-\rho)(\alpha_x + \alpha_y) + \beta_x + \beta_y] \\
B_3 &= \tfrac{1}{2}(\alpha_y\beta_x - \alpha_x\beta_y)
\end{aligned} \tag{30}$$

For all three values of ρ, $|G|$ is again greatest when $\alpha_x = \alpha_y$, $\beta_x = \beta_y$, and $\theta_x = \theta_y = \pi$, which yields the constraint given by Equation (26) needed to preserve numerical stability as $\beta_x, \beta_y \to \infty$. Equation (26) also applies to the method of Bell *et al.* [9] and is equivalent to the stability requirement of the LW and Fromm schemes when applied to the pure advection equation. However, it is much more restrictive than the corresponding requirement for the WB scheme for pure advection, which is $\alpha_x + \alpha_y \leqslant 2$. The limit imposed by Equation (26) arises because of the explicit treatment of diffusion in the predictor equation. As previously mentioned, Minion [11] proposed a modification of the Bell *et al.* model to obtain the stability limit,

$$\alpha_x, \alpha_y \leqslant 1 \tag{31}$$

This modification requires the computation of an additional pseudo concentration field at the cell faces that is used to compute the predictor advection terms perpendicular to the cell faces.

Although this approach is conditionally stable for $\beta_x, \beta_y \to \infty$, the implicit treatment of diffusion in both dimensions requires the inversion of a pentadiagonal matrix in order to obtain the solution of the governing equation. This is much more computationally expensive than inverting a tridiagonal matrix as is needed in one-dimensional problems. The situation becomes worse in three dimensions or solving the governing equation on a curvilinear grid. In geophysical applications, the vertical dimension is much smaller than the horizontal dimensions and as a result, the vertical grid spacing is typically much smaller than the horizontal grid spacing. The previous analysis showed that the explicit treatment of vertical diffusion, in combination with a small grid spacing, requires the use of a small time step to preserve numerical stability. Therefore, a more efficient method might be to treat vertical diffusion implicitly to obtain better numerical stability and treat horizontal diffusion explicitly to avoid inverting a pentadiagonal matrix and therefore improve computational efficiency. This method is now investigated.

Semi-implicit method 2

Assume x is a horizontal direction and diffusion in this direction is treated explicitly, while y is the vertical direction and diffusion is treated implicitly in this direction. The predictor is now computed as

$$\begin{aligned} & c_{j,k}^{n+1/2} - \frac{w\beta_y}{2}(c_{j,k+1}^{n+1/2} - 2c_{j,k}^{n+1/2} + c_{j,k-1}^{n+1/2}) \\ & \quad = c_{j,k}^{n} - \tfrac{1}{2}(\alpha_x \Delta_x c_{j,k} + \alpha_y \Delta_y c_{j,k}) \\ & \qquad + \frac{\beta_x}{2}(c_{j+1,k}^{n} - 2c_{j,k}^{n} + c_{j-1,k}^{n}) + \frac{\tilde{w}\beta_y}{2}(c_{j,k+1}^{n} - 2c_{j,k}^{n} + c_{j,k-1}^{n}) \end{aligned} \tag{32}$$

The corrector is

$$\begin{aligned} & c_{j,k}^{n+1} - \frac{\beta_y}{2}(c_{j,k+1}^{n+1} - 2c_{j,k}^{n+1} + c_{j,k-1}^{n+1}) \\ & \quad = c_{j,k}^{n} - \alpha_x(c_{j+1/2,k}^{n+1/2} - c_{j-1/2,k}^{n+1/2}) - \alpha_y(c_{j,k+1/2}^{n+1/2} - c_{j,k-1/2}^{n+1/2}) \\ & \qquad + \beta_x(c_{j+1,k}^{n+1/2} - 2c_{j,k}^{n+1/2} + c_{j-1,k}^{n+1/2}) + \frac{\beta_y}{2}(c_{j,k+1}^{n} - 2c_{j,k}^{n} + c_{j,k-1}^{n}) \end{aligned} \tag{33}$$

A Von Neumann analysis of this method results in the following:

$$\begin{aligned} [1 + \beta_y(1 - \cos\theta_y)]G = {} & A_0 + A_1\cos\theta_x + A_2\cos\theta_y + A_3\cos 2\theta_x \\ & + A_4\cos 2\theta_y + A_5\sin\theta_x + A_6\sin\theta_y + [B_0 + B_1\sin\theta_x + B_2\sin\theta_y \\ & - A_3\sin 2\theta_x - A_4\sin 2\theta_y + B_3\cos\theta_x + B_4\cos\theta_y]I \end{aligned} \tag{34}$$

with

$$A_0 = 1 - \left(\frac{1-3\rho}{2} + \tilde{A}\right)(\alpha_x + \alpha_y) - 2\tilde{A}\beta_x - \beta_y$$

$$A_1 = \alpha_x(1-2\rho) + (\alpha_x + 2\beta_x)\tilde{A} \quad A_2 = \alpha_y(1-2\rho+\tilde{A}) + \beta_y$$

$$A_3 = \frac{\alpha_x}{2}(\rho - 1) \quad A_4 = \frac{\alpha_y}{2}(\rho - 1) \quad A_5 = \alpha_x\tilde{B} \quad A_6 = \alpha_y\tilde{B}$$

$$B_0 = -\tilde{B}(\alpha_x + \alpha_y + 2\beta_x) \quad B_1 = \alpha_x(\rho - \tilde{A} - 1) \quad B_2 = \alpha_y(\rho - \tilde{A} - 1) \tag{35}$$

$$B_3 = \tilde{B}(\alpha_x + 2\beta_x) \quad B_4 = \tilde{B}\alpha_y$$

$$\tilde{A} = \frac{1 + \tilde{\rho}(\alpha_x + \alpha_y) - \beta_x - \tilde{w}\beta_y + [\beta_x - \alpha_x\tilde{\rho}]\cos\theta_x + [\tilde{w}\beta_y - \alpha_y\tilde{\rho}]\cos\theta_y}{1 + w\beta_y(1 - \cos\theta_y)}$$

$$\tilde{B} = -\frac{\alpha_x \sin\theta_x + \alpha_y \sin\theta_y}{2[1 + w\beta_y(1 - \cos\theta_y)]}$$

where $\tilde{\rho} = \rho - \frac{1}{2}$.

For $w = 0$ and all ρ, the maximum value of $|G|$ occurs when $\alpha_x = \alpha_y$ and $\theta_x = \theta_y = \pi$, which results in the following stability constraints:

$$\beta_x < \tfrac{1}{2} \tag{36}$$

$$\alpha_x + \alpha_y \leqslant 1 - 2\beta_x \tag{37}$$

and for $\beta_x > 0$, Equation (37) is more restrictive than the method 1 constraint given by Equation (26).

For $w = 1$ and all ρ, the maximum value of $|G|$ also occurs when $\alpha_x = \alpha_y$ and $\theta_x = \theta_y = \pi$, which results in the stability constraint given by Equation (26). However, this model is also unstable for other cases unless Equation (37) is obeyed. Therefore, treating diffusion implicitly in the predictor does not yield as much of an advantage as implicitly integrating stiff source terms as previously illustrated.

PHASE AND AMPLITUDE ERRORS

When modelling mass transport in rivers, lakes, and coastal regions, the lateral extent of the domain may be a kilometre or more, while the water depth is typically several metres or less. Model resolution is usually limited by computational resources to a lateral spacing on the order 100 m or more and a vertical spacing of a fraction of a meter or more. Typical lateral flow velocities in such shallow water bodies are primarily on the order of 1 m/s or less while vertical velocities are often two orders of magnitude smaller or even negligible. Therefore, it is reasonable to assume $\alpha_x = \alpha_y$. The vertical turbulent diffusivity varies due to bed roughness and has been estimated in the range of 0.0001–0.001 m^2/s, while the lateral diffusivity is typically 2–10 times as large [14]. Therefore a reasonable assumption is that $\beta_y = 100\beta_x$. However,

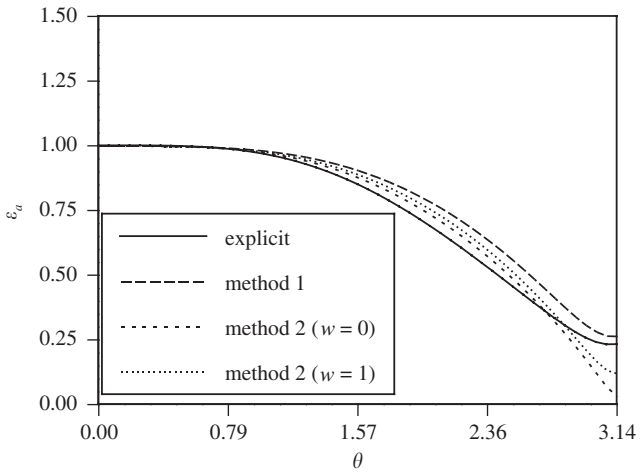

Figure 4. ε_a for the LW methods for $\beta_x = 0.01$ and $\beta_y = 0.1$.

under this assumption, methods 1 and 2 yield virtually identical predictions so therefore it is assumed that $\beta_y = 10\beta_x$. Furthermore, it is assumed that $\alpha_x = \alpha_y = 0.4$, $\beta_x = 0.01$, $\beta_y = 0.1$, and for simplicity, $\theta_x = \theta_y$. The relative amplitude error is defined as the ratio of the numerical to the exact solution amplitudes, i.e.

$$\varepsilon_a = \frac{|G|}{e^{-0.11\theta^2}} \tag{38}$$

while the relative phase error is similarly defined as the ratio of the numerical and exact phases,

$$\varepsilon_p = \frac{\tan^{-1} B/A}{0.8\theta} \tag{39}$$

For this example, the grid Peclet number in the x direction, $\mathbf{Pe}_x = \alpha_x/\beta_x = 40$ while in the y direction, $\mathbf{Pe}_y = 4$. For $\mathbf{Pe}_y \approx 100$, advection dominates the solution and the treatment of vertical diffusion does not affect the accuracy of the solution. Figure 4 shows a plot of ε_a for the different LW methods, which reveals that all of the methods perform similarly, but the semi-implicit methods are more accurate than the explicit method for all but the largest θ. Figure 5 shows the corresponding plots of ε_p and illustrates that the explicit method has the least error for small θ and possesses a leading phase error for larger θ. The semi-implicit methods have a lagging error for all but the largest values of θ and method 2 with $w = 0$ has the smallest error of all the semi-implicit schemes.

Figures 6 and 7 show plots of ε_a and ε_p for the different variations of the WB method. All of the methods perform similarly and overpredict modes and have a leading phase error for large θ. Once again methods 1 and 2 with $w = 0$ perform similarly. Figures 8 and 9 show plots of ε_a and ε_p for the Fromm methods. These models are a blend of the LW and WB methods and their errors reflect this. In this case, the explicit method is slightly more dissipative than the semi-implicit methods and has a leading phase error for large θ. The semi-implicit methods also exhibit a leading phase error, but to a much lesser degree.

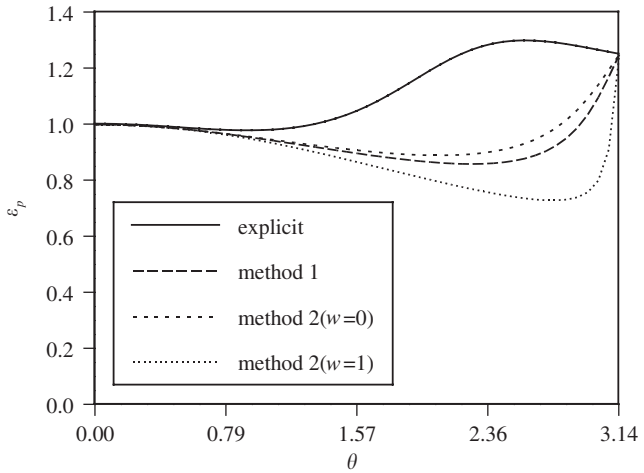

Figure 5. ε_p for the LW methods for $\beta_x = 0.01$ and $\beta_y = 0.1$.

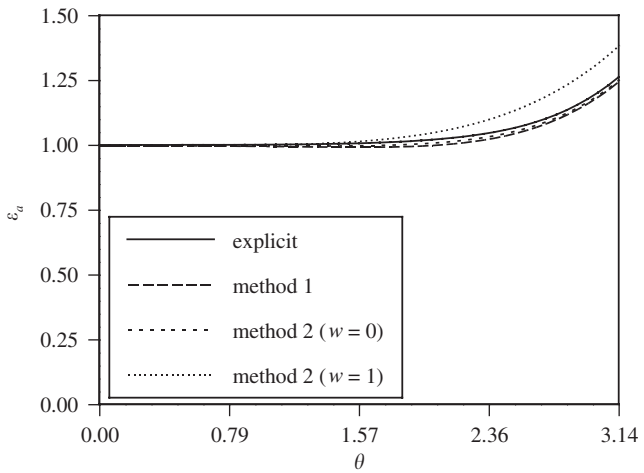

Figure 6. ε_a for the WB methods for $\beta_x = 0.01$ and $\beta_y = 0.1$.

Although methods 1 and 2 are conditionally stable for large β_y, they are not necessarily accurate. To illustrate this, the relative amplitude and phase errors are computed with the same parameters as the previous case except now $\beta_x = 0$ and $\beta_y = 0.5$ are used. In this case, methods 1 and 2 with $w = 0$ are identical and therefore results for method 2 only are presented. Figures 10 and 11 show ε_a and ε_p for the LW versions of method 2 with $w = 0$ and $w = 1$. Both schemes greatly overpredict the solution and possess a severe lagging error for increasing θ. Figures 12 and 13 show ε_a and ε_p for the WB models, which demonstrate that they overpredict the solution and have a leading phase error for larger θ. The amplitude and phase errors for the Fromm models are shown in Figures 14 and 15. Both versions overpredict the solution,

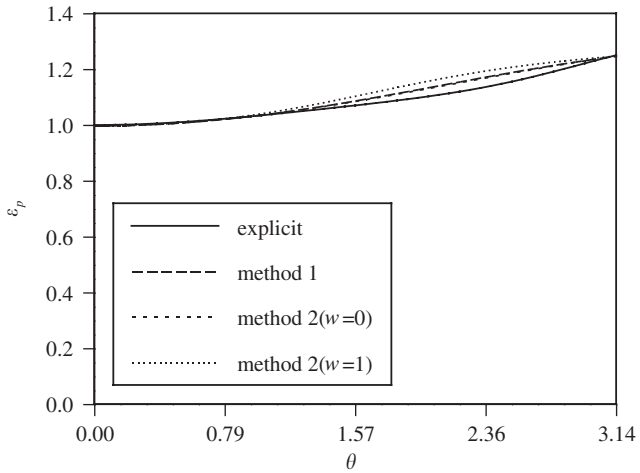

Figure 7. ε_p for the WB methods for $\beta_x = 0.01$ and $\beta_y = 0.1$.

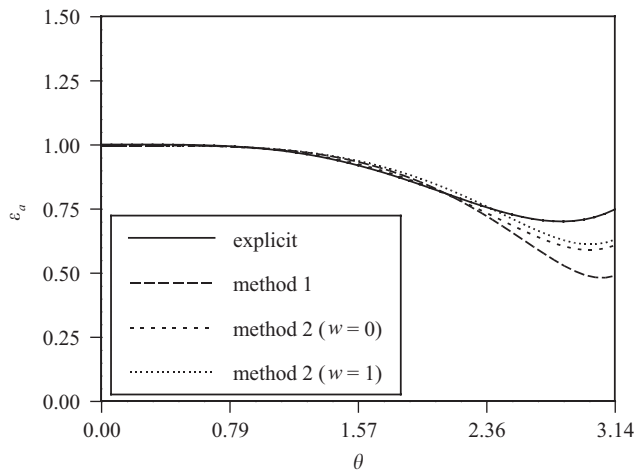

Figure 8. ε_a for the Fromm methods for $\beta_x = 0.01$ and $\beta_y = 0.1$.

but the version with $w = 0$ has a lagging phase error and the version with $w = 1$ has a leading phase error. Fortunately, for large values of β_y both methods are still dissipative ($|G| < 1$) and therefore stable.

COMPUTATIONAL EXAMPLES

Three idealized problems are now solved by the explicit and semi-implicit versions of the Fromm models in order to compare their predictions with analytical solutions. Only method 2

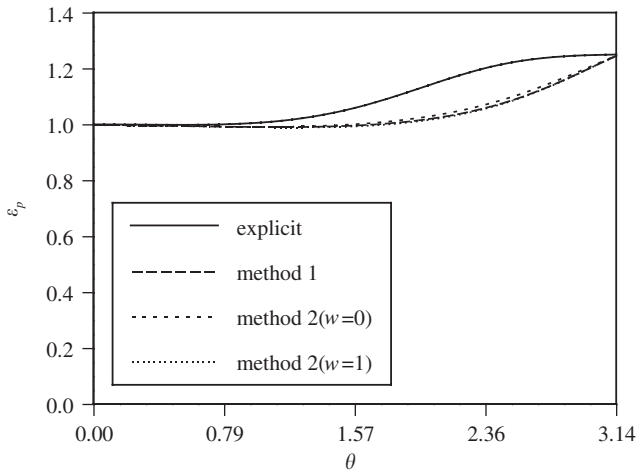

Figure 9. ε_p for the Fromm methods for $\beta_x = 0.01$ and $\beta_y = 0.1$.

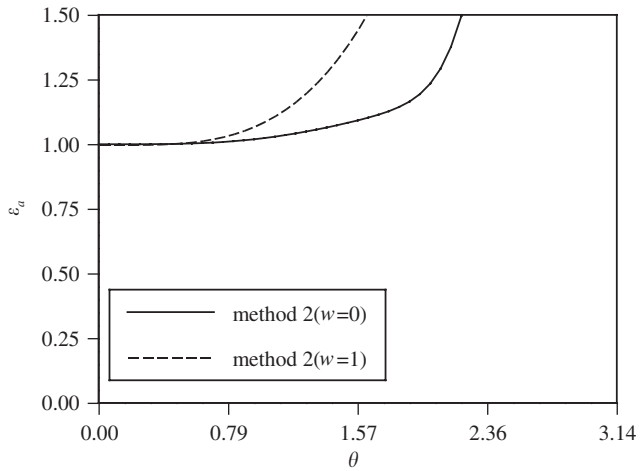

Figure 10. ε_a for the semi-implicit LW methods for $\beta_x = 0$ and $\beta_y = 0.5$.

with $w = 0$ is utilized in these computations. As previously mentioned, method 1 requires the inversion of a pentadiagonal matrix, which is accomplished by using a preconditioned biconjugate gradient scheme [13]. An ADI method would be computationally cheaper, but would sacrifice second-order time accuracy when coupled with the Crank–Nicolson method in each dimension [14]. Method 2 requires the inversion of a tridiagonal matrix that is accomplished with the standard Thomas Algorithm. In the first two problems, the domain consists of a 1000 m long channel with a 10 m depth. The first problem is designed to mimic a geophysical flow in which vertical advection is negligible and the chosen parameters are $u = 0.5\,\mathrm{m/s}$, $v = 0$, $D_x = 0.01\,\mathrm{m^2/s}$, and $D_y = 0.001\,\mathrm{m^2/s}$. At the top and bottom boundaries, $c = 0$ is enforced, while

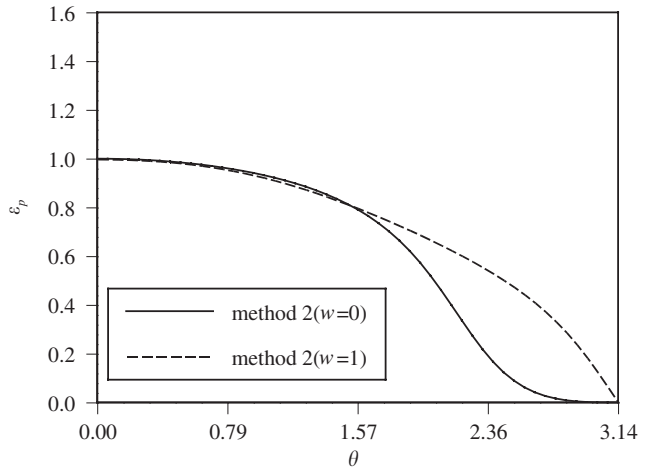

Figure 11. ε_p for the semi-implicit LW methods for $\beta_x = 0$ and $\beta_y = 0.5$.

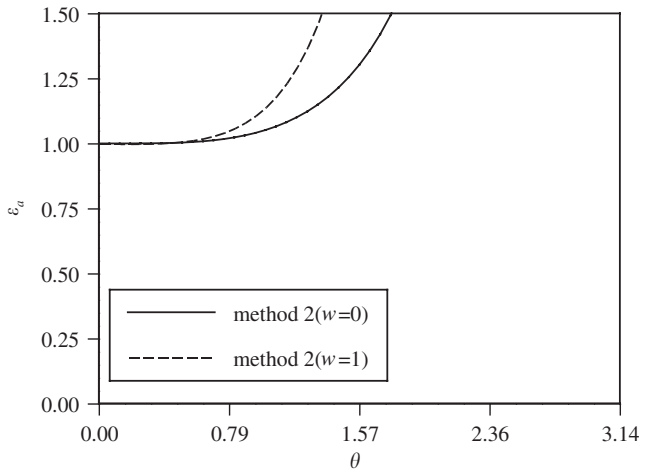

Figure 12. ε_a for the semi-implicit WB methods for $\beta_x = 0$ and $\beta_y = 0.5$.

at the right boundary $\partial c/\partial x = 0$ and at the left boundary the following is specified:

$$c(0, y) = \frac{y}{25}(10 - y) \tag{40}$$

The models are run with varying grid resolution as shown in Table I to obtain a steady-state solution that is compared to the analytical result. All of the models yielded nearly identical solutions for all three problems. Figure 16 shows the convergence of the predictions to the analytical solution along $y = 5$ m for a varying number of computational cells, N. Figure 17 shows the corresponding profiles for $x = 500$ m.

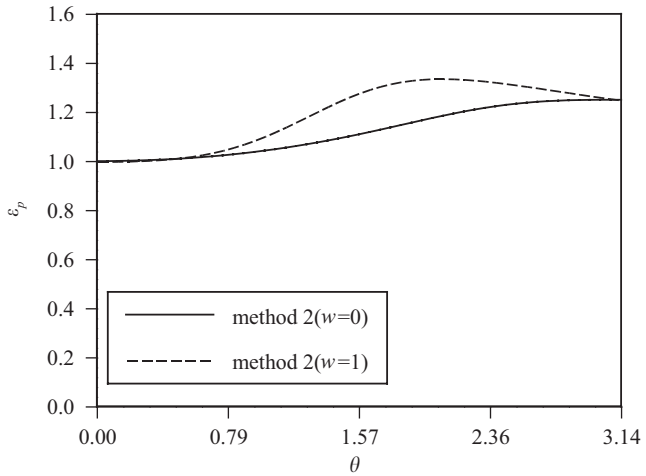

Figure 13. ε_{p} for the semi-implicit WB methods for $\beta_x = 0$ and $\beta_y = 0.5$.

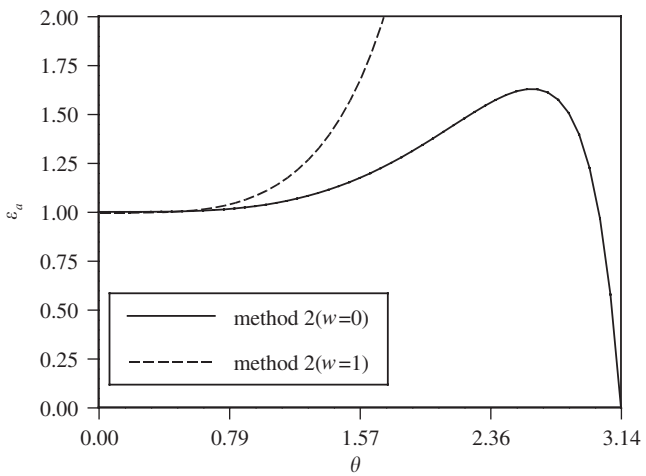

Figure 14. ε_{a} for the semi-implicit Fromm methods for $\beta_x = 0$ and $\beta_y = 0.5$.

The second problem is designed to illustrate the case where c represents turbulence kinetic energy or its dissipation rate. In such a case, $c = 0$ is enforced at the surface and c at the bottom is fixed to some positive value based on the local shear stress. In this case, it is assumed to be,

$$c(x, 0) = \sin^2 \frac{\pi x}{1000} \tag{41}$$

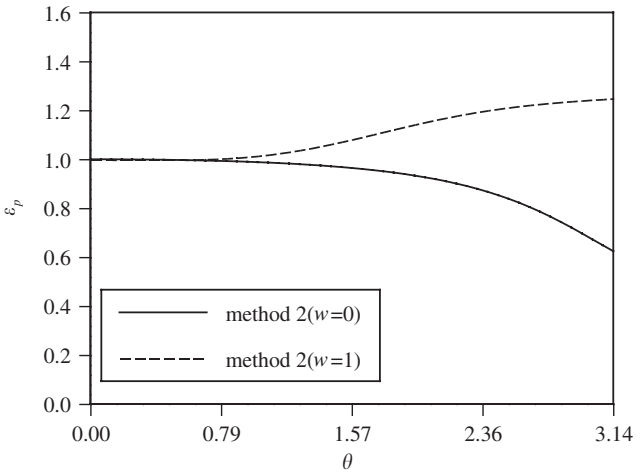

Figure 15. ε_p for the semi-implicit Fromm methods for $\beta_x = 0$ and $\beta_y = 0.5$.

Table I. Comparison of computational effort for the semi-implicit Fromm methods relative to the explicit Fromm method.

Grid	Δx	Δy	Δt	α_x	β_x	β_y
1	100	1	100	0.5	0.0001	0.1
2	50	0.5	50	0.5	0.0002	0.2
3	25	0.25	25	0.5	0.0004	0.4
4	12.5	0.125	7.1	0.3	0.00046	0.45

Also, at the left and right boundaries, $c = 0$ is specified. Lateral advection is neglected to facilitate comparison with the analytical solution and the parameters are now $u = 0$ and $v = 0.01$ m/s, with D_x and D_y the same as before. Table II shows the various grid resolutions used in this example. Figure 18 shows the predictions and analytical solution along $y = 5$ m for a varying number of computational cells. Figure 19 shows the corresponding plots along $x = 500$ m. In this case, a boundary layer exists near the surface and a sharp gradient of c in the y direction exists.

The third example is an unsteady problem in which a mass of tracer equal to $C_0 \Delta x \Delta y$ (where $C_0 = 1$ is the initial concentration) is released from the computational cell located 100 m from the left boundary and 1 m from the bottom. In this case, the domain is 2000 m long and 20 m deep and at the left and right boundaries $\partial c/\partial x = 0$ is enforced, while at the top and bottom $\partial c/\partial y = 0$ is applied. The parameters are now $u = 0.5$ m/s and $v = 0.005$ m/s, with D_x and D_y the same as before and Table III shows the grid parameters for this problem. Figure 20 shows the analytical solution at $t = 2000$ s, while Figure 21 shows the corresponding numerical solution.

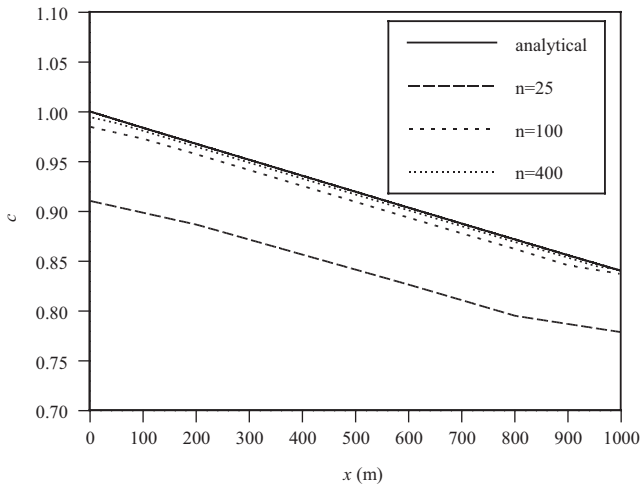

Figure 16. Comparison of numerical predictions to analytical solution for test problem 1 along $y = 5\,\mathrm{m}$.

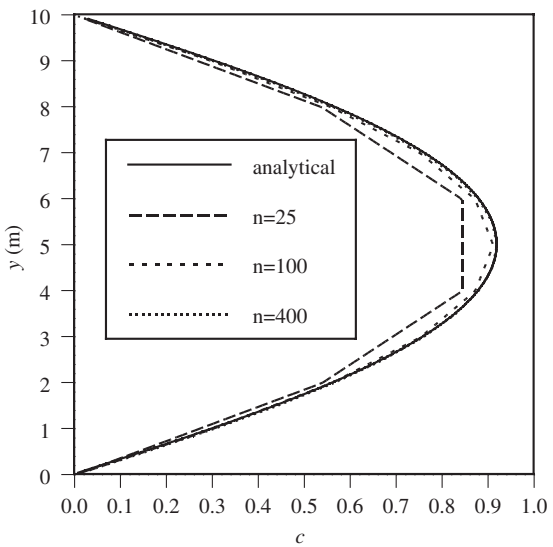

Figure 17. Comparison of numerical predictions to analytical solution for test problem 1 along $x = 500\mathrm{m}$.

Figure 22 shows the L_2 error norm for the models as a function of the number of computational cells, N, which is computed as

$$L_2 = \sqrt{\frac{1}{N}\sum_{i=1}^{N}(c_{\mathrm{exact}} - c_{\mathrm{predict}})^2} \tag{42}$$

Table II. Comparison of computational effort for the semi-implicit Fromm methods relative to the explicit Fromm method.

Grid	Δx	Δy	Δt	α_x	β_x	β_y
1	100	1	100	0.5	0.00005	0.05
2	50	0.5	50	0.5	0.0001	0.1
3	25	0.25	25	0.5	0.0002	0.2
4	12.5	0.125	6.25	0.5	0.0004	0.4
5	6.25	0.0625	1.9	0.3	0.0005	0.49

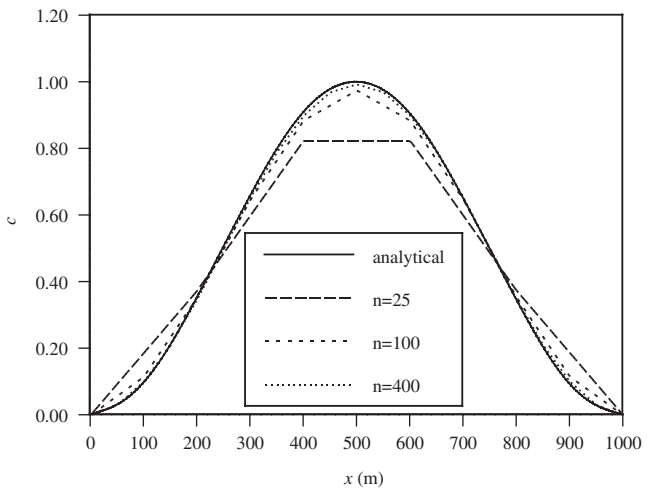

Figure 18. Comparison of numerical predictions to analytical solution for test problem 2 along $y = 5\,\mathrm{m}$.

This figure reveals that the methods converged at a constant rate until roundoff errors and boundary effects reduced the rate. The model predictions were less accurate in case 2 than case 1 because of the severe boundary layer at the surface, which caused an abrupt variation of c and hindered convergence. In addition, there is more error in case 3 than in case 1 due to the dominance of advection in the x direction that causes a sharp gradient in c at the front of the plume.

Although these models yield nearly identical solutions, the corresponding computational effort is quite different. For coarse grids where the limiting timestep is governed by the Courant condition, Equation (26), the explicit method is the fastest. However, as the grid is refined, explicit model stability becomes governed by diffusion, Equation (23). The ratio of the diffusion limiting timestep, Δt_{d}, to the Courant limiting timestep, Δt_{C}, can provide a rough delineation of when this occurs,

$$\frac{\Delta t_{\mathrm{d}}}{\Delta t_{\mathrm{C}}} = \frac{u\Delta y}{2D_y}\,\frac{\Delta y}{\Delta x} \tag{43}$$

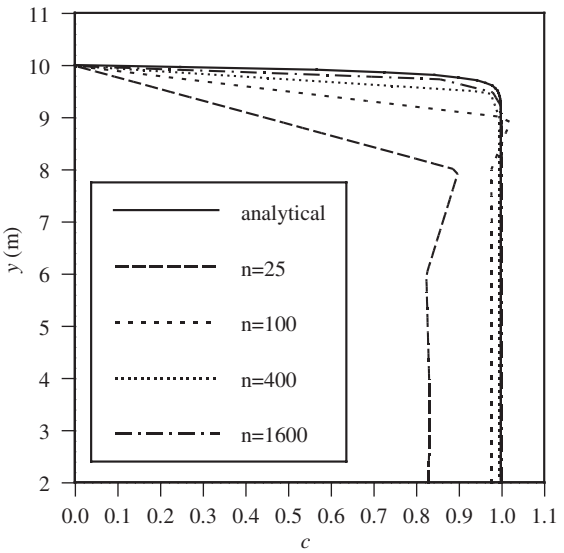

Figure 19. Comparison of numerical predictions to analytical solution for test problem 1 along $x = 500$m.

Table III. Comparison of computational effort for the semi-implicit Fromm methods relative to the explicit Fromm method.

Grid	Δx	Δy	Δt	α_x	α_y	β_x	β_y
1	50	0.5	33.33	0.33	0.33	0.00013	0.13
2	25	0.25	16.67	0.33	0.33	0.00027	0.27
3	12.5	0.125	6.67	0.267	0.267	0.00043	0.43
4	6.25	0.0625	1.67	0.133	0.133	0.00043	0.43

When this ratio is equal to one, then further reduction of Δy will force the explicit model to use a smaller timestep than the semi-implicit models to maintain stability. For the problems considered here with $u = 0.5$ m/s, $D_y = 0.001$ m^2/s, and $\Delta y/\Delta x = 0.01$, then Δy must be less than approximately 0.4 m before the semi-implicit methods gain an advantage over the explicit method. Furthermore, the ratio given in Equation (43) can be used to crudely estimate the relative computational effort of method 2 versus the explicit method. For example, for the given parameters and $\Delta y = 0.0625$ m, method 2 could use a time step 6.4 times as large as the explicit method, which can be roughly translated to 84 per cent less CPU time. This is further illustrated for the finest grid simulations of the three test problems. Table IV shows the relative CPU time, which is the CPU time divided by the explicit method CPU time, for the finest grid simulation of each problem. This reveals that method 1 is 5–10 times as costly to use as the explicit method, while method 2 is only approximately 1.3 times as costly when using the same Δt. However, methods 1 and 2 are not limited by vertical diffusion and can therefore use a larger Δt and still remain stable. For example, in the first

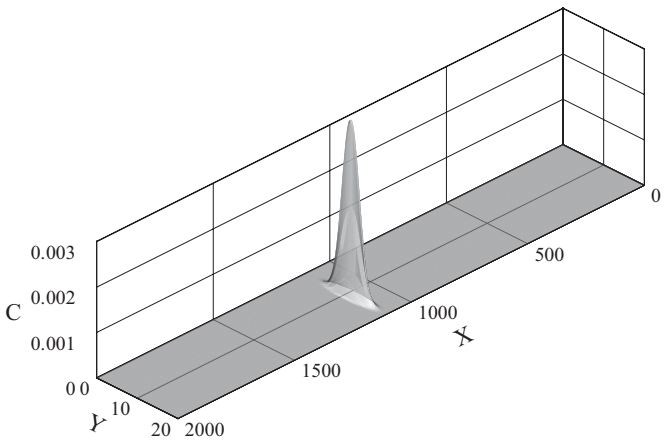

Figure 20. Analytical solution to test problem at $t = 2000$ s.

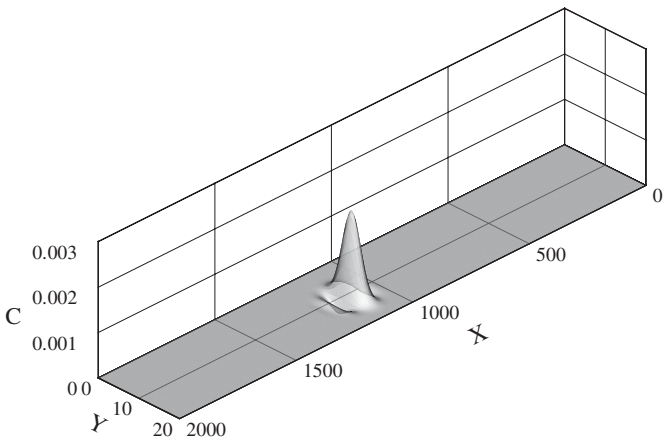

Figure 21. Numerical solution to test problem at $t = 2000$ s.

problem, method 1 using $\Delta t = 12.5$ s still required 6.4 times as much CPU time as the explicit method. However, using this timestep, method 2 required only 0.74 times as much CPU time as the explicit model or a 26 per cent reduction. An even larger Δt could be employed for additional efficiency. In problem 2, using $\Delta t = 3.125$ s, method 2 required 0.81 times as much CPU time, a 19 per cent reduction. Finally, in the third case, method 2 using $\Delta t = 4.1675$ s required 0.52 times as much CPU time as the explicit model or a 48 per cent reduction. In all three cases, the use of a larger timestep with the semi-implicit methods had a negligible impact on accuracy.

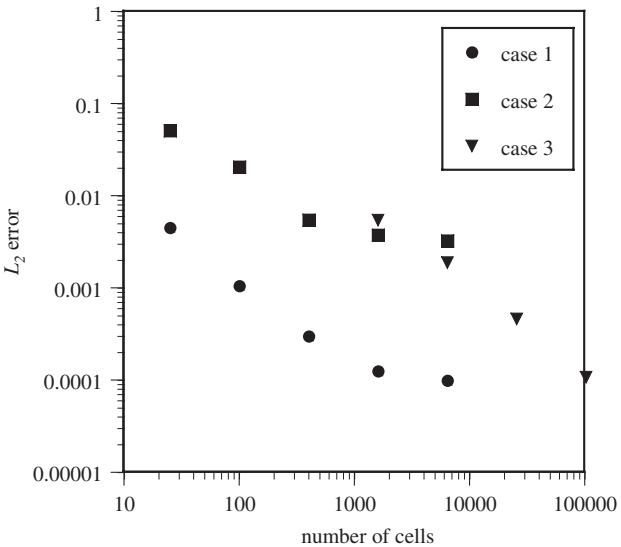

Figure 22. L_2 error norm for all test problems.

Table IV. Comparison of computational effort for the semi-implicit methods relative to the explicit method.

Case	Method 1	Method 2
1	10.1	1.38
2	10.56	1.32
3	5.38	1.38

SUMMARY AND CONCLUSIONS

The semi-discrete analysis of the proposed semi-implicit method illustrates the benefit of treating stiff source terms implicitly when computing the predictor as well as the corrector solutions. This benefit consists of a much enlarged stability region for all γ that is much larger than the corresponding regions of the ABCN and ASIRK-2 semi-implicit methods.

The Von Neumann analysis presented in this paper reveals that for a low **Pe** (less than 100), the choice of time integration technique for the diffusion terms has a modest effect on the amplitude and phase accuracy of the numerical solution. The LW schemes showed the most sensitivity, while the WB schemes were the least sensitive. Also, for the test case presented, the Fromm and LW semi-implicit schemes are more accurate than the explicit version, while the opposite is true for the WB method. For a **Pe** on the order of 100 or greater, advection dominates the solution and the treatment of diffusion makes no significant difference in the overall accuracy of the models.

However, the time integration choice does affect the efficiency and robustness of the numerical model. The explicit treatment of diffusion requires the use of a smaller timestep than

the semi-implicit methods when the ratio given by Equation (43) is less than one. The implicit integration of diffusion in all spatial directions eliminates this constraint, but requires the inversion of large, sparse, matrices that are computationally expensive to perform. In the test problems presented here, this method still required several times the computational effort of the explicit model despite its ability to use larger timesteps. Only in cases with a large β_x is this method justified. Selectively treating vertical diffusion implicitly is an attractive compromise that enhances the stability and robustness of the model, limits matrix inversion to tridiagonal matrices, and does not compromise the accuracy of the model. In the test problems, this method required 20–50 per cent less CPU time than the explicit method. It was also discovered that unlike the treatment of stiff source terms, implicitly treating vertical diffusion when computing the predictor does not significantly enhance the overall stability of the model.

REFERENCES

1. Ollivier-Gooch C, Van Altena M. A high-order accurate unstructured mesh finite-volume scheme for the advection–diffusion equation. *Journal of Computational Physics* 2002; **181**:729–752.
2. Wood WA, Kleb WL. Diffusion characteristics of finite volume and fluctuation splitting schemes. *Journal of Computational Physics* 1999; **153**:353–377.
3. Zwart PJ, Raithby GD, Raw MJ. The integrated space-time finite volume method and its application to moving boundary problems. *Journal of Computational Physics* 1999; **154**:497–519.
4. Leveque RJ, Yee HC. A study of numerical methods for hyperbolic conservation laws with stiff source terms. *Journal of Computational Physics* 1990; **86**:187–210.
5. Moin P, Kim J. On the numerical solution of time-dependent viscous incompressible fluid flows involving solid boundaries. *Journal of Computational Physics* 1980; **35**:381–392.
6. Verwer JG, Blom JG, Hundsdorfer W. An implicit-explicit approach for atmospheric transport-chemistry problems. *Applied Numerical Mathematics* 1996; **20**:191–209.
7. Knoth O, Wolke R. Implicit-explicit Runge–Kutta methods for computing atmospheric reactive flows. *Applied Numerical Mathematics* 1998; **28**:327–341.
8. Zhong X. Additive semi-implicit Runge–Kutta methods for computing high-speed nonequilibrium reactive flows. *Journal of Computational Physics* 1996; **128**:19–31.
9. Bell JB, Colella P, Glaz HM. A second-order projection method for the incompressible Navier–Stokes equations. *Journal of Computational Physics* 1989; **85**:257–283.
10. Van Leer B. Towards the ultimate conservative difference scheme. V. A second order sequel to Godunov's method. *Journal of Computational Physics* 1979; **32**:101–136.
11. Minion ML. On the stability of Godunov-projection methods for incompressible flow. *Journal of Computational Physics* 1996; **123**:435–449.
12. Fischer HB, Imberger J, List EJ, Koh RCY, Brooks NH. *Mixing in Inland and Coastal Waters*. Academic Press: New York, 1979.
13. Press WH, Teukolsky SA, Vetterling WT, Flannery BP. *Numerical Recipes in Fortran*. Cambridge University Press: New York, 1992.
14. Hirsch C. *Numerical Computation of Internal and External Flows*. Wiley: New York, 1990.

